J Mater Sci (2015) 50:3883–3894
DOI 10.1007/s10853-015-8907-2

Comparison between the ferroelectric/electric properties of the $PbZr_{0.52}Ti_{0.48}O_3$ films grown on Si (100) and on STO (100) substrates

Cristina Chirila · Andra Georgia Boni · Iuliana Pasuk · Raluca Negrea · Lucian Trupina · Gwenael Le Rhun · Shi Yin · Bertrand Vilquin · Ioana Pintilie · Lucian Pintilie

Received: 21 August 2014 / Accepted: 10 February 2015 / Published online: 14 March 2015
© Springer Science+Business Media New York 2015

Abstract Ferroelectric/electric properties of $PbZr_{0.52}Ti_{0.48}O_3$ (PZT) thin films grown by pulsed laser deposition (PLD) on two different substrates, Si (001) and $SrTiO_3$ (STO) (001), were comparatively analyzed. The structural characterization has revealed the epitaxial relationship between the grown layers and the two types of substrates, with larger density of structural defects for the films deposited on Si (001) with buffer STO layer. The ferroelectric/electric properties are also different, with lower remnant polarization (about half of the value obtained on STO substrate), higher dielectric constant (about two times larger), and lower leakage current (about two orders of magnitude lower) for the PZT films deposited on Si (001) compared to those deposited on (001) STO substrates. Nevertheless, the results show that the use of a STO buffer layer on Si can be a solution to obtain good quality PZT capacitor structures without using expensive single-crystal oxide substrates. In this way, applications based on PZT capacitors (e.g. non-volatile memories, pyroelectric detectors, light switches, etc.) would be more easily integrated directly on Si wafers.

C. Chirila (✉) · A. G. Boni · I. Pasuk · R. Negrea · L. Trupina · I. Pintilie · L. Pintilie
National Institute of Materials Physics, Atomistilor 105bis, 77125 Magurele, Ilfov, Romania
e-mail: dragoi@infim.ro

A. G. Boni
Faculty of Physics, University of Bucharest, 077125 Magurele, Romania

G. Le Rhun · S. Yin
CEA, LETI, MINATEC Campus, 17 rue des Martyrs, 38054 Grenoble Cedex 9, France

S. Yin · B. Vilquin
INL, CNRS UMR5270, Ecole Centrale de Lyon, Université de Lyon, 36 avenue Guy de Collongue, 69134 Ecully Cedex, France

Introduction

Ferroelectrics, in capacitor geometry, are intensely used for applications such as non-volatile memories (NVM), infrared (IR) pyroelectric detectors, piezoelectric transducers, or micromechanical systems (MEMS) [1]. Perovskite $Pb(Zr_xTi_{1-x})O_3$ (PZT) is one of the most studied materials for applications due to its very good ferroelectric, piezoelectric, and pyroelectric properties. For a Zr/Ti ratio of 52/48, this material is near the morphotropic phase boundary and it is known to exhibit very good piezoelectric properties [2, 3]. Thin films of PZT with Zr/Ti ratio of 52/48 are studied for sensors and actuators applications because they have a high electro-mechanical coupling factor due to existence of both rhombohedral and tetragonal phases [4, 5].

The ferroelectric/electric properties of a thin film can be affected by the compositional and structural defects such as impurities, vacancies, grain boundaries, secondary phases, etc. Many of these defects, with extrinsic contributions to the ferroelectric/electric properties, can be eliminated by the epitaxial growth of the PZT films using pulsed laser deposition (PLD) [6, 7]. Previous reports show that epitaxial films can have superior properties compared to polycrystalline ones [8, 9]. Therefore, a lot of effort was done to obtain high quality epitaxial layers [10]. However, high quality PZT films are usually obtained on single-crystal substrates with perovskite structure, such as $SrTiO_3$ (STO) or $DyScO_3$ (DyScO). Eventually, the strain in the film can be adjusted by controlling the mismatch between the lattice constants of the PZT film and of the substrate.

This can have a significant impact on the ferroelectric properties such as remnant polarization and coercive field [11–13]. The integration of the above mentioned applications (memories, sensors, etc.) with the semiconductor technology requires the deposition of the PZT layer on Si wafers. Metal–ferroelectric–semiconductor structures, with PZT as the ferroelectric and Si as the semiconductor material, were tested for ferroelectric field effect transistors but it was found that the PZT-Si interface is compromised by the formation of silicates and other parasitic phases [14]. Thin layers of other insulating materials (e.g. MgO, SiO_2, yttrium stabilized ZrO_2, STO) were used as barriers against inter-diffusion, allowing the growth of PZT on the Si wafers [15–18]. However, the lack of free charges in the insulating layers, necessary to compensate the depolarization field in the ferroelectric, has impact on the magnitude of the remnant polarization leading to poor retention properties in a memory cell based on metal–ferroelectric–insulator–semiconductor structures [19]. Therefore, it appears that the integration of ferroelectric capacitors directly on Si is more suitable for applications. It means that, besides the buffer layer used to adjust the lattice mismatch between Si and PZT, a conductive layer has to be deposited prior the PZT growth, preferably with the same perovskite structure as the PZT [20, 21].

In this work, we perform a comparative study of ferroelectric $PbZr_{0.52}Ti_{0.48}O_3$ (PZT) thin films grown by PLD method on the Si (001) and STO (001) substrates. On Si substrate a STO buffer layer was deposited by molecular beam epitaxy (MBE), acting as a template for PZT deposition and as a barrier for Pb diffusion into Si [22–24]. Additionally, a 20 nm layer of $SrRuO_3$ (SRO) was grown by PLD on top of the STO film in order to act as back electrode for metal-ferroelectric-metal capacitors [10]. It is found that, although the polarization of the PZT film grown on single-crystal STO substrate is still superior, the PZT films deposited on STO-buffered Si wafers posses polarization of comparable value. On the other hand, it is found that the leakage current in the PZT films deposited on Si substrate is of about two orders of magnitude lower than for those deposited on STO substrate. These findings could be important for further integration of PZT capacitors in Si technology, especially for IR detectors and MEMS systems directly connected to the electronic circuitry processing the signals.

Experimental part

PZT thin films with SRO buffer layer were prepared using PLD on STO (001) and Si (001) substrates. An STO buffer layer was deposited by MBE on Si, the growth details can be found in Refs. [25, 26]. A KrF excimer laser (248 nm, 27 ns duration, 5 Hz) was line-focused onto a target rotating at 25 rpm. The SRO and PZT targets have been bought from Praxair. The fluence of the laser beam was set at 2 J/cm^2 (about 350 mJ/pulse). The substrate target distance was set at 60 mm. An accurate control of the oxygen pressure in the deposition chamber and of the substrate temperature during the growth process allow us to obtain good SRO and PZT thin films. In the case of SRO layer, the substrate temperature was increased at 700 °C and the oxygen pressure was set at 0.133 mbar. For the PZT layer deposition, the temperature was decreased at 575 °C and the oxygen pressure was set at 0.2 mbar. After the PZT deposition the films were annealed in 1 bar of O_2, for 1 h, in order to compensate the oxygen vacancies. The epitaxial relationship between deposited layers was investigated by X-ray diffraction (XRD) using a Bruker D8 Advance diffractometer with nickel-filtered copper radiation ($K\alpha 1 = 1.5406$ Å, $K\alpha 2 = 1.5444$ Å) and a parabolic X-ray mirror for beam collimation at the X-ray tube output. The measurements were performed in coplanar geometry with horizontal sample stage which means that the incident and the diffracted beams are always in-plane with the normal to the sample stage, and spinning of the sample during phi-scans is allowed only around the vertical axis. The analytical transmission electron microscopy (TEM) and high resolution transmission electron microscopy (HRTEM) investigations have been performed with a JEM ARM 200F analytical microscope with C_S corrector on the probe mode. The cross-section specimens for TEM observations have been prepared by mechanical polishing followed by ion milling at low angle in a Gatan PIPS installation. Ferroelectric properties at microscale level were tested by performing piezoelectric force microscopy (PFM) with a MFP-3D-SA model microscope from Asylum Research. In order to investigate the ferroelectric properties of the PZT layer at macroscale level, Pt electrodes with 0.01 mm^2 area were deposited on the top surface by magnetron sputtering, using a shadow mask. The polarization–voltage (P–V) measurements were performed using a TF2000 ferritester system equipped with a FE-Module (aixACCT), while the capacitance–voltage (C–V) characteristic were recorded using a Hioki LCR meter. The current–voltage (I–V) characteristics were raised by using a Keithley 6517 electrometer with incorporated dc voltage source. The temperature measurements were performed in a Lake Shore cryoprober model CPX-VF with CuBe needles.

Results

Structural characterization

The XRD patterns of the PZT thin films grown on the two different substrates are shown comparatively in Fig. 1a.

The analysis showed the textured growth of the layers, and did not reveal extra-phases. The lattice parameter of the STO substrate (cubic, s.g. Pm-3m) determined experimentally was $a = 3.9050$ Å, and that of the Si substrate (cubic, s.g. Fd-3m) was $a = 5.4307$ Å. These values agree well with the reference data [27, 28]. The substrate's peak positions were used as internal reference points for the out-of-plane lattice constants for both samples as well as for the reciprocal space mapping (RSM) in the case of the film on the STO substrate.

The insert in Fig. 1a points upon the layer fringes (f) that appear around the diffraction peaks of both samples. These are related to the SRO layer in the case of the PZT/SRO/STO structure and to both STO and SRO in the case of the PZT/SRO/STO/Si structure. In the last case, the regularity of the SRO fringes is perturbed by the superposition with the STO fringes, the two layers having comparable thicknesses. The presence of layer fringes proves the good crystalline quality of SRO and STO thin films as well as the flatness of the interfaces, both being characteristic to the epitaxial growth. The crystal quality of PZT was investigated by omega-scans based on the PZT 002 lines (Fig. 1b). The degree of alignment of the PZT crystal planes was found to be significantly better in the film grown on STO single crystal.

Azimuth-scans (phi-scans) were performed on tilted crystal planes in order to prove the single-crystal-like orientations of the oxide layers and to determine their relative in-plane orientations (Fig. 1c)—the phi-scans of PZT/SRO/STO are not shown). The occurrence of four maxima, related to the fourfold rotation axis of the pseudo-cubic structures, confirm the epitaxial growth of the layers. The phi-scans analysis shows that the relative in-plane orientations are such that PZT[100]//SRO[100]//STO[100]//Si[110], which means that the epitaxial growth of STO on Si is driven by the matching $a_{Si} = 5.4307$ Å $\approx a_{STO}\ 2^{1/2} = 5.5225$ Å, with the mismatch $(a_{STO}\ 2^{1/2} - a_{Si})/a_{Si} = 1.7$ %.

The 2θ-ω scans in Fig. 1a show that the out-of-plane lattice parameter of PZT is significantly larger for the layer grown on STO substrate ($c_{PZT} = 4.113$ Å), compared to the one grown on Si (4.055 Å). The reference data for bulk tetragonal $PbZr_{0.52}Ti_{0.48}O_3$ are $a = 4.0460$ Å, $c = 4.1394$ Å [5].

RSM were constructed in the vicinity of the (−103) nodes of STO, SRO, and PZT in order to determine the in-plane lattice constants (Fig. 2). These revealed that PZT grown on Si is nearly cubic ($a_{PZT} = 4.069$ Å, $c_{PZT} = 4.055$ Å), while PZT on STO has a more elongated unit cell ($a_{PZT} = 4.040$ Å, $c_{PZT} = 4.113$ Å). One can note in Fig. 2b the asymmetry of the intensity levels around the PZT node suggesting a spreading of the PZT lattice constants towards lower in-plane and higher out-of-plane lattice constants, therefore towards a more elongated PZT cell. This might suggest that elongated tetragonal PZT domains, with the longer axis normal to the surface, are existent in this layer as a minor phase. On the other hand, in Fig. 1a, the profiles of the PZT lines at higher diffraction

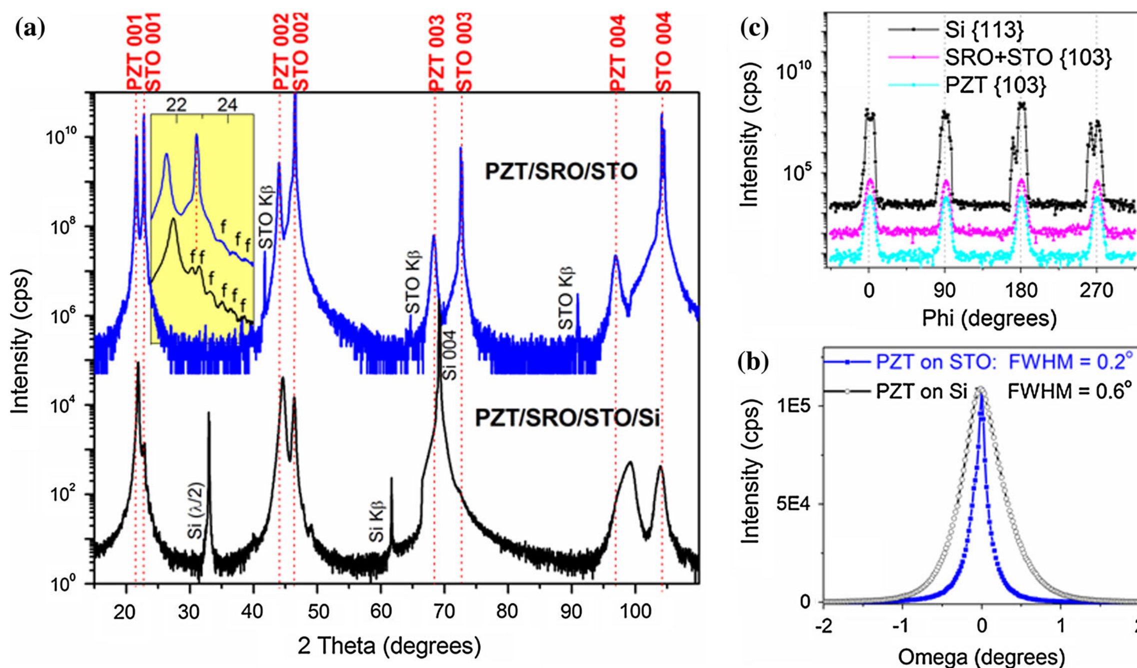

Fig. 1 **a** 2θ-ω scans; **b** PZT rocking curves around PZT 002; **c** phi-scans obtained on the PZT/SRO/STO/Si heterostructure

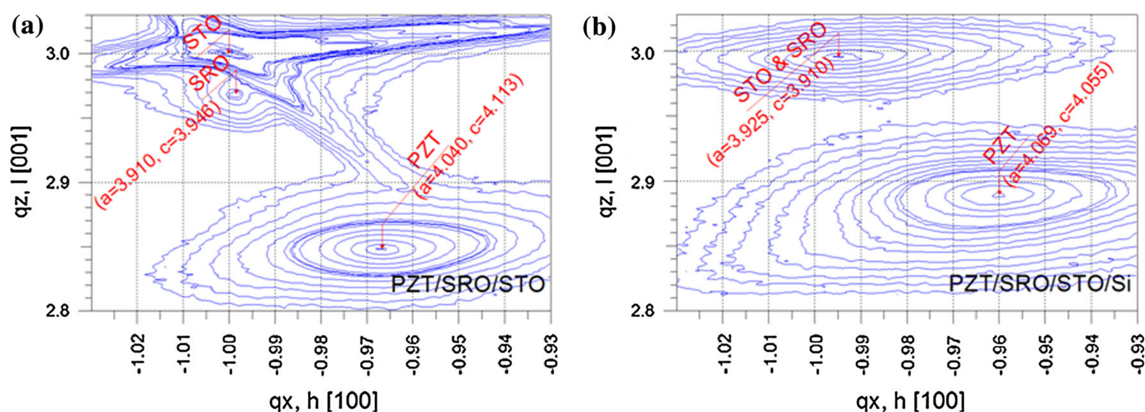

Fig. 2 Reciprocal space mappings around the (−103) nodes of STO, SRO, and PZT; **a** for PZT/SRO/STO; **b** for PZT/SRO/STO/Si. The *maps* are recorded between the same limits to facilitate visual comparison

angles of PZT/SRO/STO/Si structure, where the resolution is better, also suggest that there are domains with both orientations, *a*-domains being in majority. This kind of growth of PZT on Si is related to the structure of SRO–STO underlayers, which show abnormal large in-plane lattice constants, although the epitaxy on Si should favor lower in-plane parameter than in bulk STO. This anomaly is known and was the subject of many studies, being attributed to the presence of the amorphous SiO_2 layer between Si and STO or to the coexistence of cubic and tetragonal STO with quite different lattice parameters [25, 26]. Unfortunately, the peaks of SRO and STO for PZT/SRO/STO/Si are superimposed both in the 2θ-ω scan (Fig. 1a) and in RSM (Fig. 2b), and thus their lattice parameters cannot be distinguished.

Summarizing the results of the XRD analysis one can say that the PZT film deposited on single crystal STO substrate is relaxed, as the in-plane lattice constant is larger for PZT than for STO ($a_{PZT} = 4.040$ Å compared to $a = 3.9050$ Å for STO). Compared with the bulk PZT of the same composition, the film on STO substrate has a slightly lower in-plane lattice constant, corresponding to a compressive strain of about 0.15 %. Also the out-of-plane lattice constant is lower compared to the bulk, with about 0.65 %. This can be an effect of relaxation, leading to the formation of dislocations and to a lower out-of-plane lattice constant. The PZT deposited on Si substrate with STO buffer layer is also relaxed. Compared to the bulk, the film has a significantly larger in-plane lattice constant, corresponding to a tensile strain of about 0.6 %. The out-of-plane lattice constant is much smaller than in the bulk, with about 2 %. This suggests that polarization may be mostly in-plane, while for the PZT on single crystal STO the polarization seems to be oriented out-of-plane.

The low-magnification TEM image in Fig. 3 displays the deposited multilayers on both substrates. The PZT, SRO, and STO layers on Si substrate have a thickness of 100, 20, and 33 nm, respectively (see Fig. 3b). The image reveals a bright thin layer (4 nm) between the Si substrate and the STO layer. The amorphous nature of this layer corresponds to the native SiO_2. The thicknesses are similar for the PZT and SRO films deposited on STO single crystal substrate (see Fig. 3a. The selected area electron diffraction (SAED) patterns reveal on both structures the crystallization status of the as-deposited layers and the orientation relationship with respect to the substrate. The diffraction spots have been marked with corresponding miller indices and subscripts indicating the substrate (the strongest spots) or the as-deposited layers. The SAED images reveal the ordered single-crystal-like nature of the grown layers on both types of substrates.

The TEM images at low and high magnification (Fig. 3a) show that defects are forming at the SRO/PZT interface (misfit dislocations), suggesting that the film is at least partly relaxed. The lattice constants for the PZT film, obtained from SAED pattern (Fig. 3a), are $a_{PZT} = 4.05$ Å and $c_{PZT} = 4.10$ Å, while for STO are $a_{STO} = c_{STO} = 3.91$ Å. These values are in good agreement with those obtained by XRD.

The TEM image corresponding to PZT/SRO/STO/Si structure (Fig. 3b) reveals a strain contrast, which may be observed also in the HRTEM image, as a consequence of the mismatch dislocations [29, 30]. This distorted region inside PZT close to the SRO interface exhibits clusters of dislocations for strain relaxation, that are expected to affect electrical measurements at micro and macroscale [31–33].

The lattice constants for the PZT film, obtained from SAED pattern (Fig. 3b), are $a_{PZT} = 4.06$ Å and $c_{PZT} = 4.06$ Å, while for STO are $a_{STO} = 3.85$ Å and $c_{STO} = 3.90$ Å. Again, for the PZT layer the results are comparable with those obtained by XRD. In any case, the structural differences between the PZT layers grown on

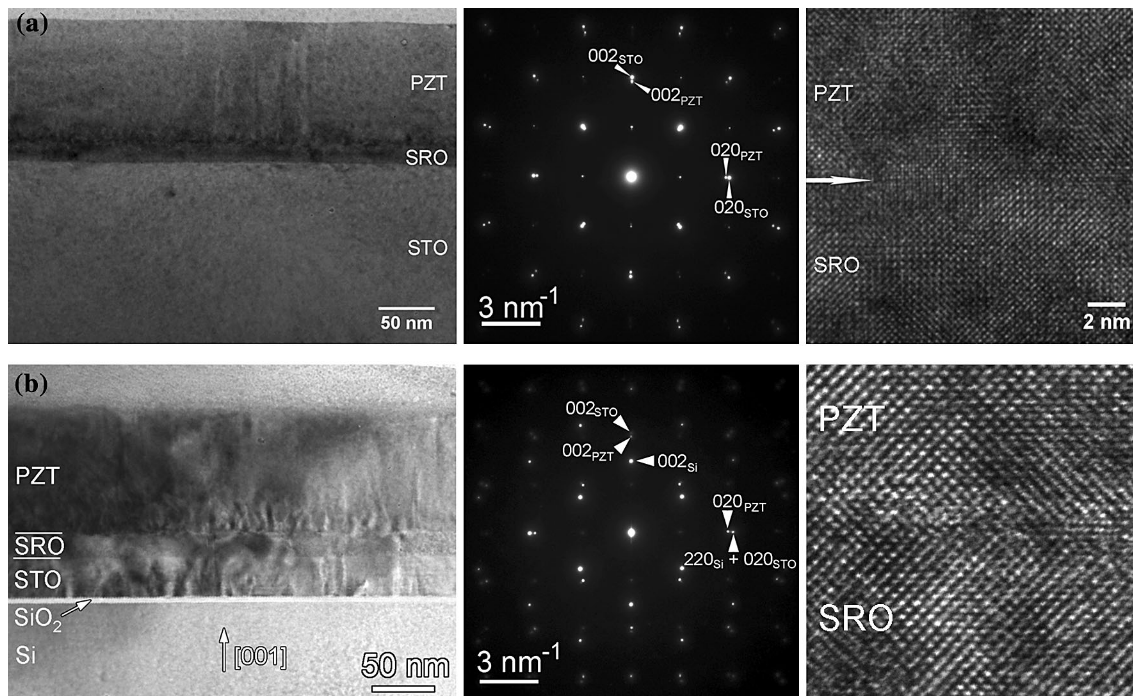

Fig. 3 **a** TEM image at low-magnification for PZT/SRO/STO structure; SAED pattern recorded on an area which includes the STO substrate and the deposited layers of SRO and PZT; HRTEM image showing the PZT-SRO interface; **b** TEM image for PZT/SRO/STO/Si structure; SAED pattern from an area which includes the Si substrate and the deposited layers of STO, SRO, and PZT; HRTEM image showing the PZT-SRO interface

single crystal STO substrate and on single crystal Si with STO buffer layer may have some impact on the electrical properties, as it will be shown later on.

The AFM analysis performed on an area of 5 × 5 μm^2 has revealed a smooth surface in both cases, with an average roughness of 1 nm ± 0.1 nm. The PFM investigation on the bare PZT surface shows little phase contrast, suggesting that most of the polarization is oriented in the same direction (see Fig. 4). A characteristic grid of 90° domains is visible for the sample grown on single crystal STO substrate (see Fig. 4a). This is in agreement with previous literature [10, 34]. Some 180° domains can be also seen for PZT on STO substrate, both in phase and amplitude. In the case of the PZT deposited on Si, the presence of domains is not evident.

The presence of switchable polarization was checked by writing artificial domains with opposite directions of polarization. The poling map is shown in the Fig. 5a. The area where a voltage of −10 V was applied on the tip is with polarization towards top surface (polarization UP) and has a light color. The area where a voltage of +10 V was applied on the tip is with polarization DOWN (towards the bottom SRO contact) and appears in a dark color in Fig. 5a, b. Comparing the colors of the phase signal in the case of the poled areas in Fig. 5 with the color for unpoled film in Fig. 4 one can have an indication for the dominant direction of polarization in the unpoled film. In the present case it seems to be UP, at least for the film deposited on STO substrate. The result is in agreement with the XRD finding that the out-of-plane lattice constant is significantly larger than the in-plane one, suggesting dominance of the out-of-plane polarization. The interpretation of the PFM results for the PZT film deposited on Si substrate, by comparing the phase signals in Figs. 4 and 5, is more difficult as the XRD results suggest a mixture of in-plane and out-of-plane polarization with some dominance of the former. This could explain the relative lack of contrast in the phase signal of the unpoled PZT film deposited on the Si substrate (see Fig. 4b). One has to mention that the dominant polarization orientation in the PZT films may depend on the strain imposed by the substrate, the film thickness, the oxygen content, etc. [35, 36] and may change in time, depending on the surrounding atmosphere and storage conditions [37].

The stability of DOWN and UP polarizations was checked by monitoring the poled areas for 120 min after the poling procedure was ended. It was found that the UP polarization is stable for both type of substrates, while the polarization DOWN has a better stability in the case of the film grown on STO substrate. This is visible by comparing the images in Fig. 5 after 30 min and after 120 min. It can be seen in Fig. 5b that the dark regions, corresponding to

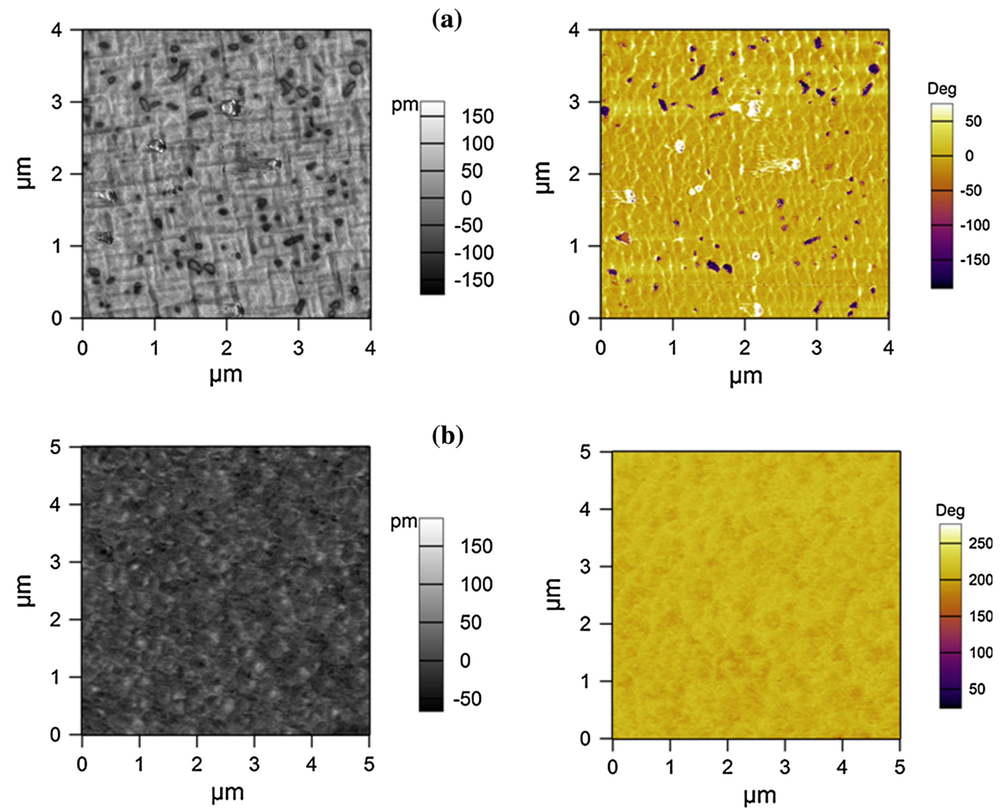

Fig. 4 PFM amplitude and phase maps for **a** PZT/SRO/STO structure; **b** PZT/SRO/STO/Si structure

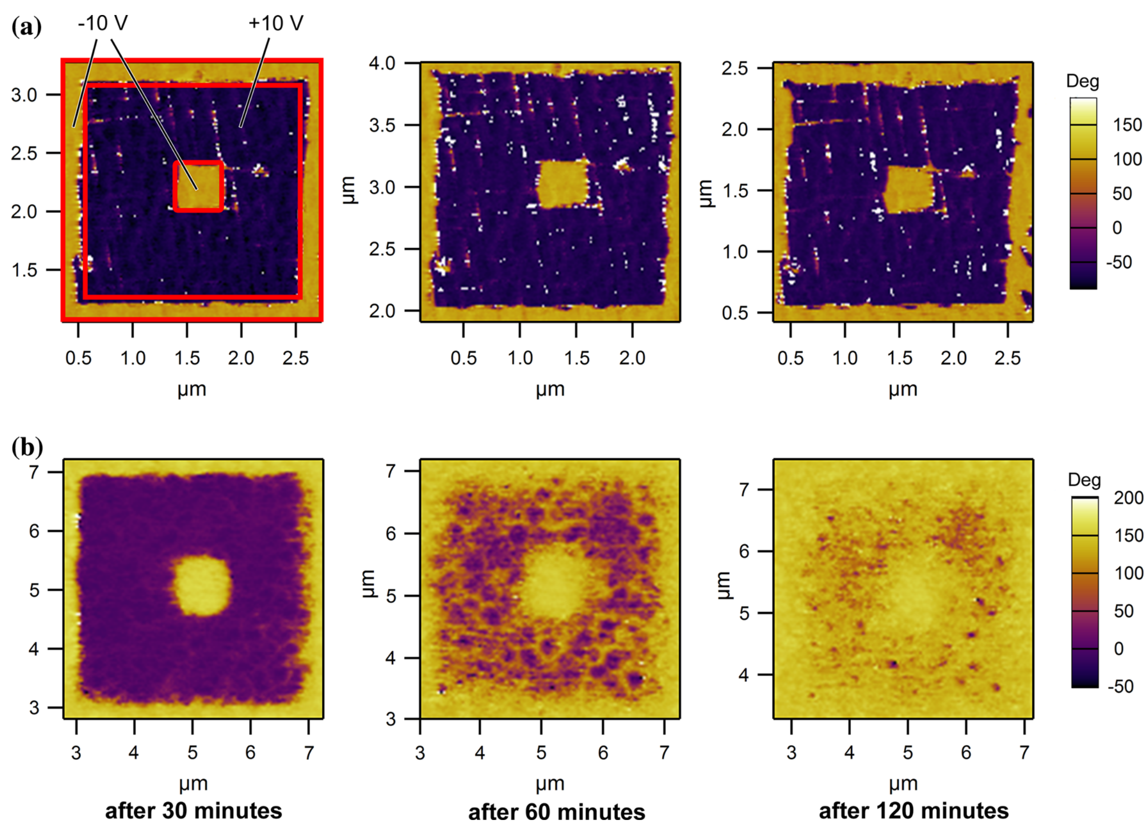

Fig. 5 The time evolution of the artificially written domains with opposite directions of polarization for **a** PZT/SRO/STO structure and **b** PZT/SRO/STO/Si structure

DOWN polarization, changes the contrast (the dark almost disappears after 120 min), while in Fig. 5a the dark regions do not change after 120 min. This result correlates well with the results of XRD investigations, showing that for the PZT film on STO substrate the out-of-plane polarization is favored. The fact that for the PZT film deposited on Si substrate one direction of polarization is not stable can be related to the more defective PZT/SRO interface in this case, as suggested by TEM investigation.

Ferroelectric/electric properties

The results of the hysteresis measurements performed at different temperatures with triangular voltage wave of 1 kHz frequency are shown in Fig. 6. Although the PZT layers deposited on Si and STO substrates are in both cases epitaxial, the P–E characteristics are different. The current loops recorded during the dynamic hysteresis measurements show peaks which are associated to the polarization reversal. The peaks for PZT/SRO/STO are sharper and thus the P–V loops obtained by integrating the I–V loops are more rectangular in this case compared to the PZT films

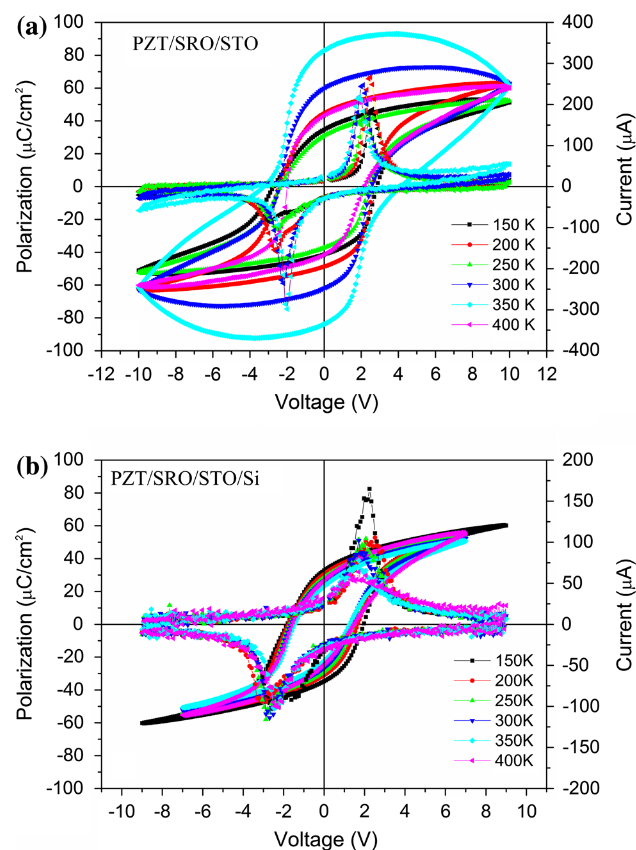

Fig. 6 Hysteresis measured at 1 kHz for **a** PZT/SRO/STO structure and **b** PZT/SRO/STO/Si structure. The characteristics were recorded in the 150–400 K temperature range

deposited on Si substrate. The values for polarization and coercive voltage, at room temperature, are of 48 μC/cm^2 and 2.5 V for PZT on single crystal STO, and of 26 μC/cm^2 and 1.3 V for PZT deposited on Si substrate with STO buffer layer. Considering that the thicknesses are about the same, one can say that the coercive field is about two times larger for the PZT deposited on STO substrate than for the film deposited on Si. In both cases the loops have a small shift towards negative voltages, of 0.05 V for PZT/SRO/STO and 0.15 V for PZT/SRO/STO/Si, suggesting the presence of an internal electric field oriented towards the bottom SRO electrode. Such a field would, apparently, favor the DOWN orientation of polarization. However, the internal field is much smaller than the coercive one, having thus, only little effect on the polarization orientation. The origin of this internal electric field will be discussed in the next section.

The shape of the hysteresis loops for PZT/SRO/STO/Si structures remains unchanged for the entire temperature range scanned in this work. However, for the PZT/SRO/STO structures the high leakage current present in these samples above 300 K (see Figs. 6a, 8a) is altering the shape of the hysteresis loops with increasing the temperature.

In Fig. 7, the dielectric constant calculated from C–V measurements performed at different temperatures are shown. These measurements were performed at 100 kHz frequency of the a.c. small signal of 50 mV amplitude. It can be seen that the different substrates have an influence on capacitance of the metal–ferroelectric–metal structure, reflected in different values of the dielectric constant. In the case of the PZT/SRO/STO/Si structure, the characteristics are symmetrical with respect to the dielectric constants values, with a small shift towards negative voltages (in agreement with the hysteresis measurements presented above). In the case of the PZT/SRO/STO substrate, there is an asymmetry in the values of dielectric constant for negative and positive polarities, with higher values and sharper peak for negative voltages. This is in accordance with the polarization hysteresis measurements where the value of the negative remnant polarization is greater than positive remnant polarization, suggesting that the polarization compensation mechanism is more effective when negative voltage is applied on the top electrode. As polarization charges are compensated with free charge carriers, it results that for negative voltages on the top electrode these carriers are responding faster leading thus to a larger capacitance value and to a larger dielectric constant (one has to remind that the capacitance measurement is related to the ability of the free carriers in respond to the small amplitude a.c. signal) [38].

Another difference between these two types of structures is related to the values of the dielectric constants as

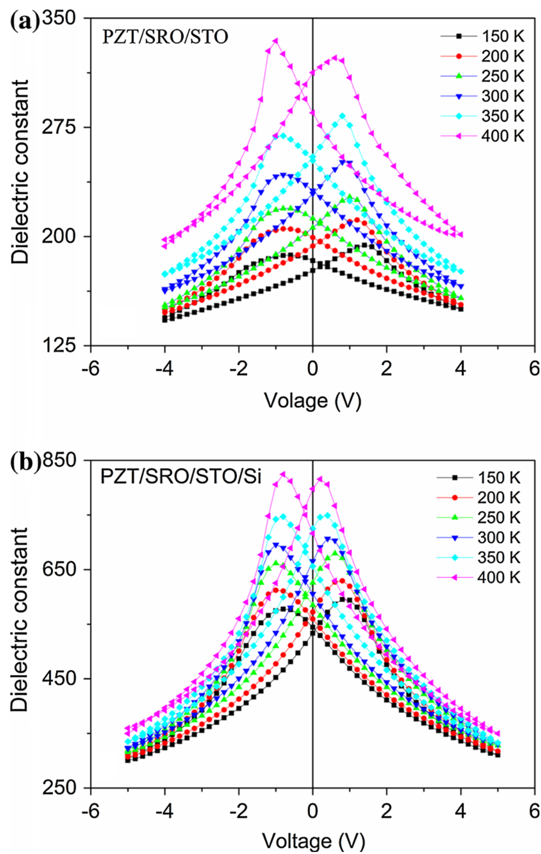

Fig. 7 The voltage dependence of the dielectric constant for **a** PZT/SRO/STO structure and **b** PZT/SRO/STO/Si structures. The characteristics were recorded in the 150–400 K temperature range

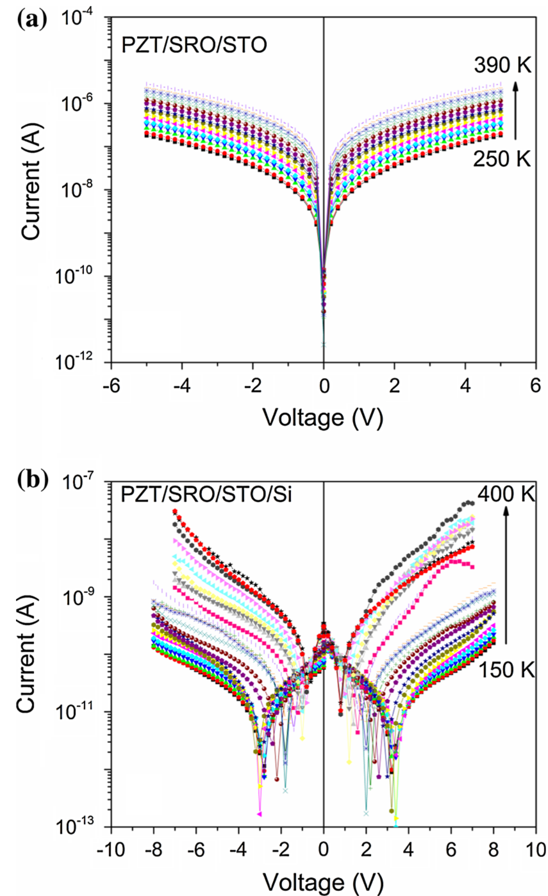

Fig. 8 I–V characteristics for **a** PZT/SRO/STO structure and **b** PZT/SRO/STO/Si structure. The characteristics were recorded in the 150–400 K temperature range

measured at the maximum applied voltage, common for both kinds of samples. Thus, at 4 V the dielectric constant of PZT/SRO/STO/Si is two times larger than that measured on PZT/SRO/STO ones. This aspect will be discussed later on.

Current–voltage characteristics have been measured for temperatures between 150 and 400 K in order to investigate the dominant conduction mechanism. The results are presented in Fig. 8 for both types of structures.

The leakage current measurements are affected by the contributions coming from polarization switching or from other transitory phenomena (e.g. releasing of trapped charge, relaxation of other polarization mechanisms not associated to ferroelectricity, etc.) [39]. The currents associated to the polarization switching are largely eliminated by poling the sample before the current measurements are performed. Then the measurement is done with voltages of the same polarity as the one used for poling, which is increased from 0 V to V_{max} in steps of 0.1 V. A 1 s delay time between changing the voltage and measuring the current is used. The delay time should be large enough to reduce the relaxation currents, but if it is too large a time-dependent breakdown could affect the measurement.

The I–V characteristics are rather symmetric with the voltage polarity and show significant temperature dependence especially for the PZT/SRO/STO/Si structure. In this case, the delay time of 1 s seems to be not enough to completely eliminate the parasitic contributions to the leakage current. This is in agreement with the hysteresis measurements presented in Fig. 6b, showing a more elongated loop for PZT/SRO/STO/Si. This can be explained by the back switching effects associated to a distribution of coercive fields [40]. In other words, for the PZT/SRO/STO structure the switching is sharp, leading to a more rectangular loop, while for PZT/SRO/STO/Si the switching is more gradual.

Discussions

The experimental results presented in the previous section show that the ferroelectric/electric properties of the PZT

films deposited on single crystal STO substrate and on Si substrate with STO buffer layer are somewhat different, due to small differences in the epitaxial quality as revealed by the structural investigations. Summarizing, the remnant polarization and the coercive field are about two times larger, the dielectric constant is about two times smaller, and the leakage current is with almost two orders of magnitude larger for the PZT film grown on single-crystal STO than for the one grown on Si with STO buffer layer. These aspects will be discussed in more detail further on.

The higher values for the remnant polarization in the case of PZT deposited on single-crystal STO substrate could be explained by different stress situations, compressive for STO substrate and tensile for Si substrate. However, previous studies have shown that the polarization value in PZT films is almost insensitive to the strain variations [41]. On the other hand it was shown that structural defects may block ferroelectric domains, leading to lower values of polarizations [42, 43]. It can be the present case, considering that the PZT film deposited on Si with STO buffer layer are more defective than the films deposited on single-crystal STO. The fact that the coercive field is higher for the PZT film deposited on single-crystal STO substrate may be related to the much higher leakage current in this case. The larger density of free carriers may screen the applied electric field [44]. As a result, higher voltages are required to switch the polarization although the thickness of the films deposited on the STO and Si substrates is about the same. Despite the lower value of the remnant polarization, the lower values for the coercive field and for the leakage current are an advantage for the PZT films deposited on Si substrate with STO buffer layers if one wants to use them for applications, as capacitors (e.g. NVM, IR detectors, etc.).

The internal electric field suggested by the shift of the hysteresis loops and C–V characteristics toward negative voltages is significantly smaller than the difference in work functions, which are of 4.6–4.9 eV for SRO and 5.65 eV for Pt [45, 46]. It is possible that the internal electric field has another origin, as for example a small gradient in the strain distribution, as suggested by TEM investigations showing misfit dislocations at the PZT/SRO interface, or a non-homogeneous distribution of some charged defects such as oxygen vacancies acting as donors [47–49]. The different distribution of strain and structural defects may also explain the increase of the dielectric constant in the case of the PZT film deposited on Si substrate with STO buffer layer. Similar results were previously reported in the literature [31–33, 50]. One has to mention here that the data presented in Fig. 7 were obtained as an independent measurement and are not derived from the data presented in Fig. 6. The C–V characteristic derived from the hysteresis loop usually leads to significantly higher values for the dielectric constant [51]. This is because the hysteresis loop was obtained by a dynamic method, integrating the charge at a frequency of 1 kHz (corresponding to 1 ms), while C–V measurement is quasi-static (slow-increasing d.c. voltage superimposed over a small amplitude a.c. signal). The contribution of the domain walls to the static dielectric constant is very much reduced in this way as the capacitance is measured for a stable value of polarization imposed by the applied d.c. voltage.

The I–V characteristics presented in Fig. 8 will be analyzed assuming that the ferroelectric capacitor can be modeled as a back-to-back connection of two Schottky type diodes [52, 53]. In this way, despite the polarity of the applied voltage on the top Pt contact, one of the diodes will be reverse biased and will limit the current. However, one cannot apply the Richardson–Schottky equation because the mean free path of the charge carriers in PZT is much smaller than the film thickness [54]. Therefore, one has to use the Schottky–Simmons equation, in which the injection is limited by the potential barriers at the electrode interfaces and the drift–diffusion in the film is limited by the carriers mobility. The Schottky–Simmons equation for the current density is given by [55, 56].

$$J = 2q\left(\frac{2\pi m_{\mathrm{eff}} kT}{h^2}\right)^{3/2} \mu E \exp\left(-\frac{q}{kT}\left(\phi_{\mathrm{B}}^{0} - \sqrt{\frac{qE_{\mathrm{m}}}{4\pi\varepsilon_0\varepsilon_{\mathrm{op}}}}\right)\right) \quad (1)$$

where J is the current density, q is the electron charge, h is the Planck's constant, m_{eff} is the effective mass, μ is the mobility, E is the electrical field in the film volume, E_{m} is the maximum electrical field at the electrode interface, k is the Boltzmann's constant, ε_0 is the vacuum permittivity, $\varepsilon_{\mathrm{op}}$ is the optical dielectric constant, ϕ_{B}^{0} is the interfacial potential barrier height at zero volts. The experimental data were analyzed using the same procedure as previously reported in the literature for ferroelectric epitaxial films with conduction mechanism dominated by thermionic emission [57, 58].

The apparent potential barrier, including the contribution of the ferroelectric polarization, is obtained from the slope of the Arrhenius plot ($\ln(J/T^{3/2}) = f(1000/T)$), as is presented in Fig. 9a for the PZT/SRO/STO structure on positive polarity. The evaluated apparent potential barrier has a linear dependence on $\sqrt{V}$ [57] as shown in Fig. 9b for the PZT/SRO/STO structure. The intercept obtained from the linear fit of the apparent potential barrier as a function of the square root of the applied voltage represents the value of the apparent potential barrier $\phi_{\mathrm{B,P}}^{0}$ at 0 V (that is a barrier reduced by the presence of the polarization charges just near the electrode interface). For the PZT/SRO/STO structure this was estimated to be 0.171 eV for

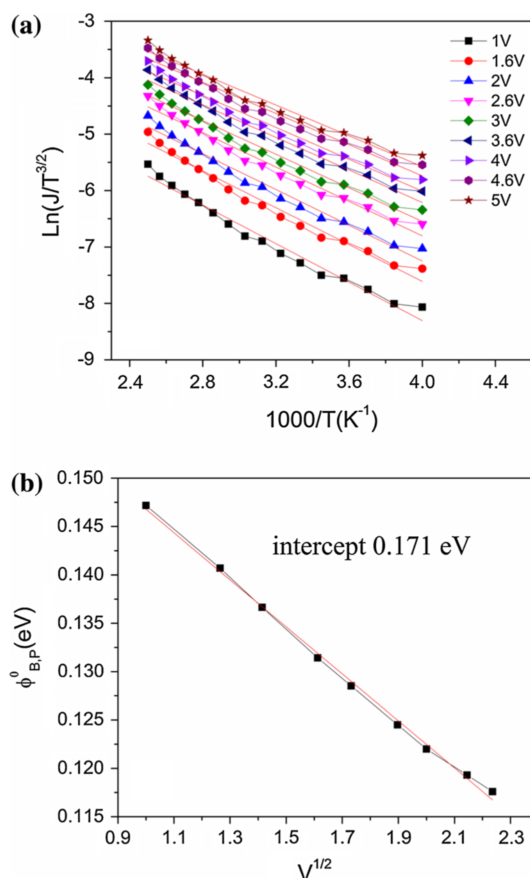

Fig. 9 **a** Arrhenius representation for positive polarity and **b** the apparent potential barrier dependence on $V^{1/2}$, analyzed for PZT/SRO/STO structure

Table 1 The substrate dependence of the remnant polarization, static dielectric constant, optical dielectric constant, apparent potential barrier, and potential barrier height

	P_r (μC/cm^2)	ε_{st}	ε_{op}	$\phi^0_{B,P}$ (eV)	ϕ^0_B (eV)
PZT/SRO/STO	50	150	8.4	0.17	0.43
PZT/SRO/STO/Si	26	300	3.9	0.27	0.46

the positive polarity and 0.175 eV for the negative polarity. In the case of PZT/SRO/STO/Si structures, the evaluated potential barriers are of about 0.27 eV. The reduction of the barrier height induced by the ferroelectric polarization is given by $\sqrt{\frac{qP}{4\pi\varepsilon_0^2\varepsilon_{op}\varepsilon_{st}}}$, where ε_{st} is the static dielectric constant. This term was estimated considering the values of remnant polarization, ε_{st} and ε_{op} given in Table 1 for PZT/SRO/STO and PZT/SRO/STO/Si structures. The value of optical dielectric constant was estimated from the slope of the $\ln(J/E) = f(E^{1/2})$ representation and the obtained values are comparable with the ones reported in literature [59]. The obtained values for the above polarization term are 0.26 and 0.19 eV for PZT/SRO/STO and PZT/SRO/STO/Si structures, respectively. Therefore, ϕ^0_B, the potential barrier height at 0 V, is around 0.45 eV for both structures.

Conclusions

Thin films of $PbZr_{0.52}Ti_{0.48}O_3$ have been deposited by PLD on STO and Si substrate. The structural characterizations comprising XRD and TEM prove an epitaxial growth on both substrates. The results of the electrical characterizations including C–V, I–V, and hysteresis measurements suggest that ferroelectric properties as remnant polarization, coercive field, dielectric constant, and leakage current are dependent on the substrate used for the deposition. The remnant polarization and the coercive field are higher for PZT deposited on single-crystal STO, while the dielectric constant is lower. However, all these qualities are of the same order of magnitude on the two types of substrates. The real advantage of the PZT films deposited on Si substrate with STO buffer layer is that they have a much smaller leakage current, almost two orders of magnitude lower compared to the film deposited on single-crystal STO substrate. This fact makes these films attractive for devices integrated directly on Si wafers.

Acknowledgements The authors acknowledge the financial support of the Romanian Ministry of Education-Executive Unit for Funding High Education, Research, Development and Innovation (MEN-UEFISCDI) through the Idea-Complex Research Grant PN-II-ID-PCCE-2011-2-0006 (contract nr. 3/2012). The authors wish to thank also Guillaume Saint-Girons, G. Niu, and Y. Robach from Institute des Nanotechnologies de Lyon Ecole Centrale de Lyon 36, Avenue Guy de Collongue 69134 Ecully, France for providing the Si substrates with the STO buffer layer deposited by MBE. Andra Georgia Boni thanks the strategic Grant POSDRU/159/1.5/S/137750, "Project Doctoral and Postdoctoral programs support for increased competitiveness in Exact Sciences research" co-financed by the European Social Found within the Sectorial Operational Program Human Resources Development 2007–2013.

References

1. Uchino K (2000) Ferroelectric devices. Marcel Dekker, New York
2. Jaffe B, Cook WR, Jaffe H (1971) Piezoelectric ceramics. Academic Press Inc, London
3. Kim DM, Eom CB, Nagarajan V, Ouyang J, Ramesh R, Vaithyanathan V, Schlom DG (2006) Thickness dependence of structural and piezoelectric properties of epitaxial $Pb(Zr_{0.52}, Ti_{0.48})O_3$ films on Si and $SrTiO_3$ substrates. Appl Phys Lett 88:142904
4. Uchino K (1996) Piezoelectric actuators and ultrasonic motors. Kluwer Academic Publishers, Boston
5. Noheda B, Gonzalo JA, Cross LE, Guo R, Park SE, Cox DE, Shirane G (2000) Tetragonal-to-monoclinic phase transition in a

ferroelectric perovskite: the structure of $Pb(Zr_{0.52}Ti_{0.48})O_3$. Phys Rev B 61(13):8687
6. Pintilie L, Vrejoiu I, Hesse D, Le Rhun G, Alexe M (2007) Extrinsic contributions to the apparent thickness dependence of the dielectric constant in epitaxial $Pb(Zr, Ti)O_3$ thin films. Phys Rev B 75(22):224113
7. Pintilie L (2009) Advanced electrical characterization of ferroelectric thin films: facts and artifacts. J Optoelectron Adv Mater 11(3):215
8. Qin M, Yao K, Liang YC (2009) Photovoltaic characteristics in polycrystalline and epitaxial $(Pb_{0.97}\ La_{0.03})\ (Zr_{0.52}Ti_{0.48})O_3$ ferroelectric thin films sandwiched between different top and bottom electrodes. J Appl Phys 105(6):061624
9. Zhu ZX, Li JF (2010) A comparative study of fibre-textured and epitaxial Nb-doped $Pb(Zr_{0.53}Ti_{0.47})O_3$ thin films on different substrates. Appl Surf Sci 256:3880
10. Vrejoiu I, Le Rhun G, Pintilie L, Hesse D, Alexe M, Gösele U (2006) Intrinsic ferroelectric properties of strained tetragonal $Pb(Zr_{0.2}, Ti_{0.8})O_3$ obtained on layer–by–layer grown, defect–free single–crystalline films. Adv Mater 18:1657–1661
11. Chen F, Tan X, Huang Z, Xuan X, Wu W (2010) Effect of electrode configurations on the process-induced imprint behavior of epitaxial Pb $(Zr_{0.52}Ti_{0.48})O_3$ capacitors. Appl Phys Lett 96:262902
12. Khan AI, Yu P, Trassin M, Lee MJ, You L, Salahuddin S (2014) The effects of strain relaxation on the dielectric properties of epitaxial ferroelectric $Pb(Zr_{0.2}Ti_{0.8})TiO_3$ thin films. Appl Phys Lett 105:022903
13. Nguyen MD, Dekkers M, Houwman E, Steenwelle R, Wan X, Roelofs A, Schmitz-Kempen T, Rijnders G (2011) Misfit strain dependence of ferroelectric and piezoelectric properties of clamped (001) epitaxial $Pb(Zr_{0.52}, Ti_{0.48})O_3$ thin films. Appl Phys Lett 99:252904
14. Zhu Y, Yan P, Yi T, Cao L, Li L (1999) Interface diffusion and chemical reaction on the interface of a PZT film/Si(111) sample during annealing treatment in N_2 and vacuum. Surf Interface Anal 27:972
15. Lin A, Hong X, Wood V, Verevkin AA, Ahn CH, McKee RA, Walker FJ, Specht ED (2001) Epitaxial growth of $Pb.Zr_{0.2}$ $Ti_{0.8}.O_3$ on Si and its nanoscale piezoelectric properties. Appl Phys Lett 78:2034
16. Basit NA, Kim HK, Blachere J (1998) Growth of highly oriented $Pb(Zr, Ti)O_3$ films on MgO-buffered oxidized Si substrates and its application to ferroelectric nonvolatile memory field-effect transistors. Appl Phys Lett 73:3941
17. Wang Y, Ganpule C, Liu BT, Li H, Mori K, Hill B, Wuttig M, Ramesh R, Finder J, Yu Z, Droopad R, Eisenbeiser K (2002) Epitaxial ferroelectric $Pb(Zr, Ti)O_3$ thin films on Si using $SrTiO_3$ template layers. Appl Phys Lett 80:97
18. Horita S, Kawada T, Abe Y (1996) Characterization of $Pb(Zr_xTi_{1-x})$ O_3 thin film on silicon Substrate with heteroepitaxial yttria-stabilized zirconia (YSZ) buffer layer. Jpn J Appl Phys 35:L1357
19. Shih WC, Juan PC, Lee JY (2008) Fabrication and characterization of metal-ferroelectric $(PbZr_{0.53}Ti_{0.47}O_3)$–Insulator (Y_2O_3)–semiconductor field effect transistors for nonvolatile memory applications. J Appl Phys 103:094110
20. Ramesh R, Gilchrist H, Sands T, Keramidas VG, Haakenaasen R, Fork DK (1993) Ferroelectric LaSrCoO/PbZrTiO/LaSrCoO heterostructures on silicon via template growth. Appl Phys Lett 63:3592
21. Eom CB, Van Dover RB, Phillips JM, Werder DJ, Marshall JH, Chen CH, Cava RJ, Fleming RM, Fork DK (1993) Fabrication and properties of epitaxial ferroelectric heterostructures with $(SrRu0_3)$ isotropic metallic oxide electrodes. Appl Phys Lett 63:2570
22. Hubbard KJ, Schlom DG (1996) Thermodynamic stability of binary oxides in contact with silicon. J Mater Res 11:2757
23. McKee RA, Walker FJ, Chisholm MF (1998) Crystalline oxides on silicon: the first five monolayers. Phys Rev Lett 81:3014
24. Reiner JW, Kolpak AM, Segal Y, Garrity KF, Ismail-Beigi S, Ahn CH, Walker FJ (2010) Crystalline oxides on silicon. Adv Mater 22:2919
25. Niu G, Saint-Girons G, Vilquin B, Delhaye G, Maurice JL, Botella C, Robach Y, Hollinger G (2009) Molecular beam epitaxy of $SrTiO_3$ on Si (001): early stages of the growth and strain relaxation. Appl Phys Lett 95:062902
26. Niu G, Penuelas J, Largeau L, Vilquin B, Maurice JL, Botella C, Hollinger G, Saint-Girons G (2011) Evidence for the formation of two phases during the growth of $SrTiO_3$ on silicon. Phys Rev B 83:054105
27. Schmidbauer M, Kwasniewski A, Schwarzkopf J (2012) High-precision absolute lattice parameter determination of $SrTiO_3$, $DyScO_3$ and $NdGaO_3$ single crystals. Acta Crystallogr B 68:8
28. Filippi C, Singh DJ, Umrigar CJ (1994) All-electron local-density and generalized-gradient calculations of the structural properties of semiconductors. Phys Rev B 50:14947
29. Hÿtch MJ, Putaux JL, Pénisson JM (2003) Measurement of the displacement field of dislocations to 0.03 Å by electron microscopy. Nature 423:27
30. Hÿtch MJ, Snoeck F, Kilaas R (1998) Ultramicroscopy 74:131
31. Choi KJ, Biegalski M, Li Y, Sharan A, Schubert J, Uecker R, Reiche P, Chen YB, Pan XQ, Gopalan V, Chen LQ, Schlom DG, Eom CB (2004) Enhancement of ferroelectricity in strained $BaTiO_3$ thin films. Science 306:1005
32. Ohno T, Ishiduka M, Arai T, Yanagida H, Matsuda T, Sakamoto N, Wakiya N, Suzuki H (2012) Strain-induced electrical properties of lead zirconate titanate thin films on a Si wafer with controlled oxide electrode structure. Jpn J Appl Phys 51:09LA13
33. Cao J, Wu J (2011) Strain effects in low-dimensional transition metal oxides. Mat Sci Eng Rep 71:35–52
34. Le Rhun G, Vrejoiu I, Pintilie L, Hesse D, Alexe M, Gosele U (2006) Increased ferroelastic domain mobility in ferroelectric thin films and its use in nano-patterned capacitors. Nanotechnology 17:3154
35. Luo Y, Li X, Chang L, Gao W, Yuan G, Yin J, Liu Z (2013) Upward ferroelectric self-poling in (001) oriented $PbZr0.2Ti0.8O_3$ epitaxial films with compressive strain. AIP Adv 3:122101
36. Dahl O, Grepstad JK, Tybell T (2009) Polarization direction and stability in ferroelectric lead titanate thin films. J Appl Phys 106:084104
37. Apostol NG, Stoflea LE, Lungu GA, Tache CA, Popescu DG, Pintilie L, Teodorescu CM (2013) Band bending at free Pb(Zr, $Ti)O_3$ surfaces analyzed by X-ray photoelectron spectroscopy. Mat Sci Eng B 178:1317
38. Schroeder DK (1998) Semiconductor material and device characterization. Wiley, New York
39. Hrib LM, Boni AG, Chirila C, Pasuk I, Pintilie I, Pintilie L (2013) Electrode interface control of the Schottky diode-like behavior in epitaxial $Pb(Zr_{0.2}Ti_{0.8})O_3$ thin films: a critical analysis. J Appl Phys 113:214108
40. Picinin A, Lente MH, Eiras JA, Rino JP (2004) Theoretical and experimental investigations of polarization switching in ferroelectric materials. Phys Rev B 69:064117
41. Lee HN, Nakhmanson SM, Chisholm MF, Christen HM, Rabe KM, Vanderbil D (2007) Suppressed dependence of polarization on epitaxial strain in highly polar ferroelectrics. Phys Rev Lett 98:217602
42. Han MG, Marshall MSH, Wu L, Schofield MA, Aoki T, Twesten R, Hoffman J, Walker FJ, Ahn CH, Zhu Y (2014) Interface-induced nonswitchable domains in ferroelectric thin films. Nat Commun 5:4693
43. Alpay SP, Misirlioglu IB, Nagarajan V, Ramesh R (2004) Can interface dislocations degrade ferroelectric properties? Appl Phys Lett 85:2044

44. Wood C, Jena D (2008) Polarization effects in semiconductors: from ab initio theory to device applications. Springer, New York
45. Hartmann AJ, Neilson M, Lamb RN, Watanabe K, Scott JF (2000) Ruthenium oxide and strontium ruthenate electrodes for ferroelectric thin-films capacitors. Appl Phys A 70:239
46. Lide DR (1995) Handbook of chemistry and physics, 76th edn. CRC, Boca Raton
47. Lo VC (2002) Modeling the role of oxygen vacancy on ferroelectric properties in thin films. Appl Phys Lett 92:6778
48. Li KT, Lo VC (2005) Simulation of oxygen vacancy induced phenomena in ferroelectric thin films. J Appl Phys 97:034107
49. Jin L, Li F, Zhang S (2014) Decoding the fingerprint of ferroelectric loops: comprehension of the material properties and structures. J Am Ceram Soc 97(1):1
50. Kim L, Jung D, Kim J, Kim YS, Lee J (2003) Appl Phys Lett 82:2118
51. Boersu I, Pintilie L, Pereira M, Vasilevskiy MI, Gomes MJM (2003) Competition between ferroelectric and semiconductor properties in $Pb.Zr_{0.65}Ti_{0.35}.O_3$ thin films deposited by sol–gel. J Appl Phys 93:4776
52. Chai FK, Brews JR, Schrimpf RD, Birnie DP III (1995) Limitations of the uniform effective field approximation due to doping of ferroelectric thin-film capacitors. J Appl Phys 78:4766
53. Delimova LA, Grekhov IV, Mashovets DV, Tyaginov SE, Shin S, Koo JM, Kim S, Park Y (2005) Transient-current measurement of the trap charge density at interfaces of a thin-film metal/ferroelectric/metal structure. Appl Phys Lett 87:192101
54. Scott JF (2000) Ferroelectric memories. Springer, Berlin
55. Simmons JG (1969) Effect of deep traps on the barrier heights of metal-insulator-metal tunnel junctions. Phys Rev Lett 23:297
56. Pintilie L, Vrejoiu I, Hesse D, LeRhun G, Alexe M (2007) Ferroelectric polarization-leakage current relation in high quality epitaxial $Pb(Zr, Ti)O_3$ films. Phys Rev B 75:104103
57. Pintilie L, Alexe M (2005) Metal-ferroelectric-metal heterostructures with Schottky contacts. Influence of the ferroelectric properties. J Appl Phys 98:124103
58. Pintilie L, Dragoi C, Chu YH, Martin LW, Ramesh R, Alexe M (2009) Orientation-dependent potential barriers in case of epitaxial $Pt–BiFeO_3–SrRuO_3$ capacitors. Appl Phys Lett 94:232902
59. Moret MP, Devillers MAC, Wörhoff K, Larsen PK (2002) Optical properties of $PbTiO_3$, $PbZr_xTi_{1-x}O_3$, and $PbZrO_3$ films deposited by metal organic chemical vapor on $SrTiO_3$. J Appl Phys 92:468